Bull. Spec. Astrophys. Obs., 2003, 56, 102-114

Speckle interferometer of the 6 m telescope

A. F. Maximov[a], Yu. Yu. Balega[a], U. Beckmann[b], G. Weigelt[b], E. A. Pluzhnik[a]

[a] Special Astrophysical Observatory of the Russian AS, Nizhnij Arkhyz 369167, Russia
[b] Max-Planck Institute fuer Radioastronomie, Bonn, D-53121, Germany

Received November 11, 2003; accepted November 15, 2003.

Abstract. A description of the 6 m telescope speckle interferometer is presented. Principles of operation and function of basic units are briefly considered. Information on the processes of observations and primary data reduction is given. Methods of measuring binary star parameters and evaluation of the power spectrum and image restoration are presented. It is shown that the use of the new device gives us an opportunity to reach acquisition rate up to 6 frames per second, and to observe objects up to 14^m with a diffraction telescope resolution of 0.″02.

Key words: instrumentation: interferometers – techniques: high angular resolution – techniques: image processing

1. Introduction

Images of celestial objects produced by ground-based telescopes are distorted because the front of the light wave passes through turbulent atmospheric layers. As distinct from aberrations of the telescope, these distortions are fast and random time variables. The effect the atmospheric turbulence has on the astronomical image quality can be substantially diminished by using interferometric properties of the telescope which manifest themselves in exposures comparable with the time of freezing of phase distortion. This idea underlies the classical method of speckle interferometry (Labeyrie 1970). The technique is based on acquisition of a series of short-exposure frames of a target and on computation of the power spectrum of objects averaged over the array. For "freezing" phase distortions, exposures from 0.01 to 01 s are used, depending on the state of the atmosphere, spectral band of the filter and characteristics of the object. The conditions of preserving coherence in each individual image require use of narrow-band interference filter. The reconstruction of images is possible within a small region of isoplanatism which does not generally exceed $1 - 2''$.

The power spectrum is calculated by summing up two-dimensional Fourier transformations of individual speckle images. For the complete reconstruction of the brightness distribution in the object, speckle interferograms of a point source are accumulated, which is used as a reference one in analyzing the spectrum. Observations of the point source are conducted under the same conditions as for the main one.

Over 20 years the 6 m telescope BTA of the Special Astrophysical Observatory of RAS has been used to carry out regular speckle interferometric observations of multiple stellar systems, measurement of angular diameters of stars and study of the structure of nuclear regions of galaxies with a limiting resolution of 0.″02. During this time several generations of devices intended for performing investigations have changed. In the present paper we describe a new speckle interferometer (hereinafter SI) designed in the Laboratory of high angular resolution methods in astronomy. A brief description of the instrument can be found on the site http://www.sao.ru./mavr/speckle/si.htm. The SI has been used for investigation with diffraction resolution of binary and multiple stars with the aim of determination of angular distances and position angles. It can also be used to perform the following tasks:

- determination of the brightness difference between the components of multiple stars in the selected spectral bands;
- measurement of angular diameters and brightness distribution over the disk of the closest giant stars;
- study of small bodies of the Solar system;
- investigation of the structures of gaseous-dust envelopes at different stages of evolution;
- investigation of morphology of circumnuclear regions of active galaxies.

The paper presents a brief review of the devices for speckle interferometry, gives a description of the principal units, procedures of observations, processing and reconstruction of data. The reconstruction of images is illustrated by the examples for a few multiples stars.

2. Detectors and systems for speckle interferometry

Using the first generation SI, the images at the telescope focus were recorded on photographic films. The light beam was first intensified by an image tube (IT). Further processing consisted in exposing the film to laser emission in coherent-optical installations. The obtained power spectra were then measured with a microphotometer or a coordinate-measuring device (Dudinov et al. 1979). Such system used on big telescope enabled taking photographs of stars of $3 - 4^m$. The disadvantages of this process were labor requirement and low measurement accuracy.

Television detectors operating in the photon counting mode formed the basis for the second generation SI. Transmitting tubes with great internal amplification capable to accumulate weak signal for a long time were in use. The main idea of the technique was to amplify a photoelectric image to such an extent that all hits of each recorded photon could be isolated from the readout noises of the television camera. The preliminary multiplication of images was also achieved with the aid of the IT. Both multistage IT of first generation and IT with multichannel plates MCP were employed. The light intensification amounted to $10^6 - 10^8$, which made it possible to observe stars up to 13th stellar magnitude together with the photon counters digital correlators calculating the autocorrelation function (ACF) on a real time bases were often used. This enabled supervision of the result in the process of acquisition and was a serious advantage of the given method (Balega et al. 1981).

In the 1980s attempts were made to use coordinate-sensitive detectors (CSD) with resistive wedge-band electrodes. The structure of the wedges and bands was chosen so that coding of the center of the photon even can be performed. An example of such a device is the camera MAMA (MultiAnode Microchannel Array) designed by Timothy (1983) with a system of multiple arrays for coding positions of photoelectrons. Such detectors required high amplification since the coordinate precision of detection of an event depends on the amplitude of the signal in the pulse. This was achieved by the application of the IT with three microchannel plates (so-called Z-configuration), however, the spatial resolution dropped to 60 μm FWHM (Nakajima et al. 1989). When using a single MCP with curved microchannels, the limiting resolution was 14 μm (Horch et al. 1992), but the amplification in this case was less than $10^5 - 10^6$. Attempts to improve the characteristics of the devices by this way caused considerable complications and, as a rule, degradation of the reliability of the devices themselves.

A little later, a detector with autocoding, in which direct coding of recorded photons with the aid of the mask in the Grey code (Papaliolios et al. 1985) was used. The resolution of the camera PAPA (Precision Analog Photon Address) created on the basis of such a detector was 512 × 512 elements over the field at a maximum flux of 5×10^5 photoelectrons/s. The quantum efficiency with the photocathodes of the company VARO did not exceed 2–3 %. Despite continuous upgrading of the camera electronics, the users of this facility did not manage to realize a stable uniform field. One more significant disadvantage was connected with non-linearity which arises when recording
close photon events. This non-linearity restricts considerably the possibilities of subsequent reconstruction of images with diffraction resolution.

The third generation SI received a development effort in connection with the advent of solid-body light detectors. Among them are self-scanning diode matrices, matrices based on injection of charge and charge coupled devices (CCD). By the present time, the latter have completely displaced vacuum detectors.

Until the year 1997 an SI with a light detector based on a television tube (supervidicon) with a resolution of 256 × 256 elements (Balega, Ryadchenko 1984) was employed at SAO RAS. The disadvantages inherent in this device: the small number of elements of decomposition, instability of electric parameters, noise sensitivity, impossibility of remote control — limited the areas of its application.

On the other hand, the upgrading of the CCD detectors, appearance of precision electromechanical positioners and fiber-optics communication lines, as well as the development of computer facilities enabled creation devices free from the indicated demerits. This was the reason for the development and creation of new tools described below.

3. Speckle interferometer

In speckle-interferometry astronomical images in a narrow spectral range, $\Delta/\lambda \approx r_0/D_1$, where D is the mirror diameter, r_0 is the Fried parameter ($\sim 6 - 10$ cm for BTA), need to be recorded with exposures comparable with times of 'freezing' of atmospheric phase distortion ($\sim 10ms$). To coordinate the scale in the focal plane of the telescope with the resolving power of the detector, the star images are magnified by the additional optics. Combination of large magnifications, short exposures and narrow spectral band of observations imposes stringent requirements on the detector sensitivity. To obtain a diffraction image, the rigidity of the mechanical structure, the precision of installation of the optical elements, the geometric and electric stability of the camera, protection of the electronics and communication lines from external electromagnetic interferences are important parameters. The assamblage of these fac-

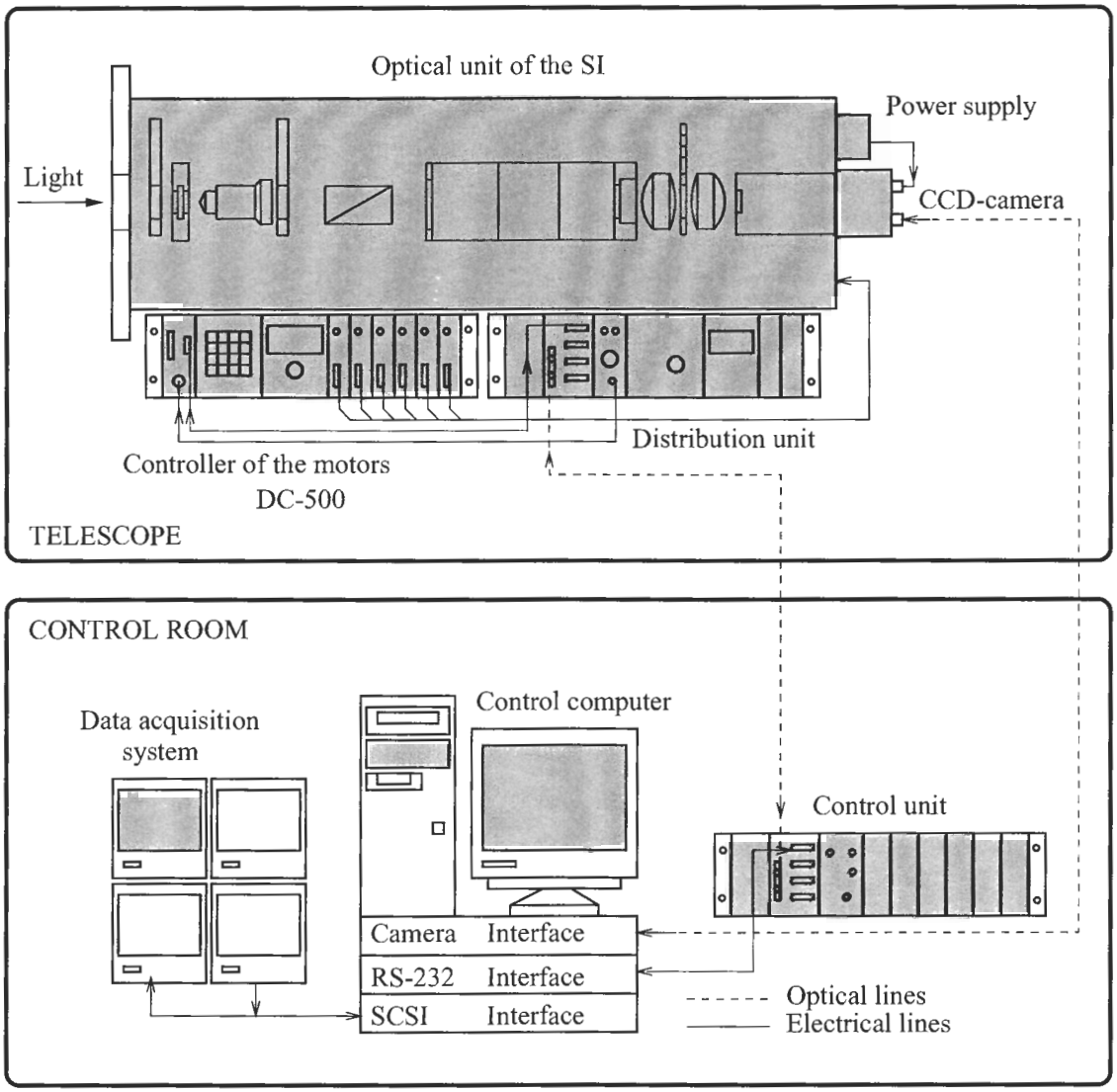

Figure 1: *Design of the speckle interferometer.*

tors determined the design features of the optical arrangement, the control and acquisition systems of the new SI.

During the observations the optical unit of the SI was housed in the prime focus cage of the telescope in accordance with the lay-out presented in Fig. 1. The other part of equipment, including the control computer and the data acquisition system, is placed in the control room. The two parts are connected by fiber-optics lines. The computer interacts with the functional units of the system via the interfaces RS-232, SCS1 and the interface of the camera SensiCam. Control is executed with the aid of the keyboard and switches located on the control unit.

The sequence of processing of the beam of light from the observed object is shown in the optical lay-out of Fig. 2.

The object image in the focal plane of the telescope is magnified by the microobjective (2) in front of which the shutter (1) that determines the exposure time is located. The interference filter (3) extracts the desired spectral band from the beam of light. The light beam passes through the prism (4) compensating atmospheric dispersion and falls on the photocathode of the image tube (5). The light-amplified image is projected from the IT display by fast objectives (6) on the matrix of the CCD camera (8). The luminosity on the matrix can be adjusted by the diaphragm (7). Now we will consider the most important SI units.

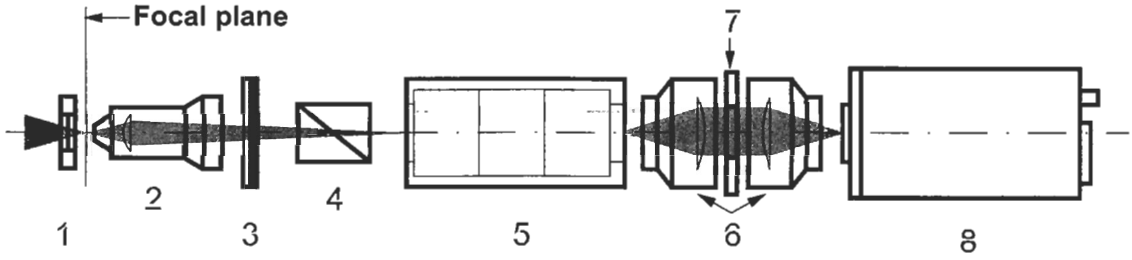

Figure 2: *Optical arrangement of the speckle interferometer.*

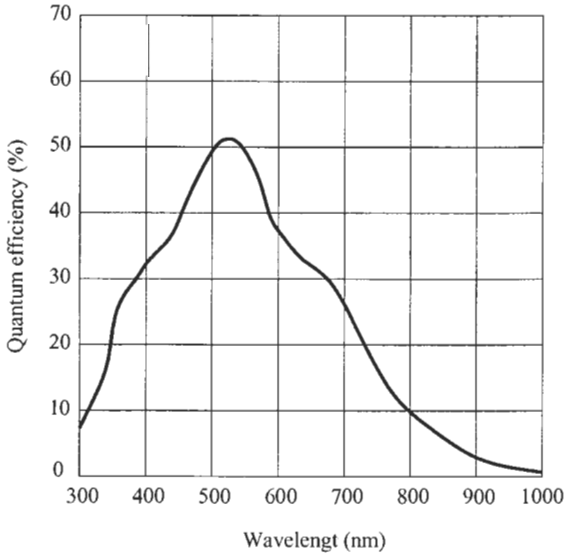

Figure 3: *Quantum efficiency of the CCD camera.*

3.1. Brightness intensifiers

For preliminary light intensification a three-sectional first-generation IT with a built-in secondary power source, fiber-optics inputs and outputs and electrostatic focusing furnished with an automatic brightness restriction system (ABS). It has a 40 mm multialcaline photocathode of type S25 and a yellow-green screen with a luminophore P20. The quantum output of the IT is about 8.3 % per 545 nm, 6.4% per 610 nm and 1.7% per 800 nm, and the maximum resolution in the center $\sim 30 mm^{-1}$. The spectral sensitivity curves of the photocathode and the relative spectral characteristics of emission of the luminophore are displayed in Fig. 4.

The light intensification coefficient in the range of illuminations on the photocathode $10^{-4} - 3 \cdot 10^{-4} lx$ is equal to about 50000. The working range of the IT is limited by the maximum illumination of $5 \cdot 10^{4} lx$. Operation with large light fluxes is prohibitive since this may cause the photometric properties of the IT to change. The facility limiting the brightness sets up an upper limit of the screen luminescence at a level of 350 cd/m^2. High voltage for the IT (45 kV) is generated by a voltage multiplier built in the housing of the device. To ensure the necessary precision, the multiplier is powered from a stabilized source of compensation type with an output voltage of 6.75 V and current up to 100 mA.

3.2. CCD camera

The light detector is the terminal element in the circuit of light-signal conversion. Information on the object of observation is displayed at the output in the digital form. Apart from high sensitivity, detector should have high homogeneity over the fild, sufficient dynamic range, minor geometric distortions.

When selecting a light detector, CCD cameras of a number of producers were analyzed: Dalsa, Proxitronic, Thompson, PCD, EEV. The device SensiCam 370LL of the PCO Computer Optics company turned out to comply best with our requirements. This model is a cooled CCD camera which provides exposures from 100 ns to 1000 s and operates in the spectral range from 280 nm to 1000 nm nm. The quantum efficiency of the camera is 53 % in the region 530 nm (Fig. 3), which is in good agreement with the maximum of radiation of the IT screen (Fig. 4).

A CCD matrix ICX085AL (SONY) with Full Frame Progressive Scan Sensor is used as a light detector. Produced by SVGA, the matrix format is 2/3″ and the resolving power 1280 × 1024 elements. Each element is a square of side 6.7 μm. A mode of unification of elements (binning) in a vertical and horizontal directions is implemented in the camera for the purpose of readout noise reduction. The reading of the matrix is performed with the use of Quiet Correlated Double Sampling, which decreases the readout noise to 8–10 electrons at a frequency of interrogation of the output register of 12.5 MHz. the matrix is provided with a two-stage thermoelectric Peltier cooler, which sets the working temperature to be −15°. This diminishes the dark current, which, in turn, makes it possible to increase the time of aquisition.

Information from the camera comes to the interface board SensiCam in the form of individual

files each of which contains one frame of the image 512×512 elements in size. The board is placed in one of the slots of the computer and interacts with the processor via PCI-bus. The time of transformation of each frame is $80\,\mu s$. With allowance made for the lag time, the rate of recording of frames into the system memory is limited by 8 frames per second. One more limitation is associated with the rate of recording on the disk through the interface SCSI and the speed of the computer. For this reason, the real recording rate is no more than 6 images per second.

The output signal of the camera represented after the conversion by the 12-bit code arrives at the input of the optical interface. Information is transmitted to the computer via a fiber-optics cable $400\,m$ long. The throughput capacity of the line is 130 Mbyte/s.

3.3. Transmitting optics

The image from the IT display is projected onto the CCD matrix on a 1:1 scale with the aid of a pair of high performance objectives produced by Rodenstock company (Germany). Their focal distance is $100\,mm$ and relative aperture 1:1.6. One of the objectives is mounted on a linear displacement unit and can move in an axial direction within $4\,mm$ to enable accurate focusing. A diaphragm intended for moderation of the light flux in observing bright objects is swung between the objectives into the parallel beam. The diaphragm has three round openings with the values 1:2.5, 1:4 and 1:8.

3.4. Matching optics

In the visible part of the spectrum the limiting spatial frequency for the 6 meter mirror at the prime focus of the telescope corresponds to a linear scale of $2\,\mu m$. According to the Nyquist theorem

$$V_{max} = \frac{1}{2l},$$

where l is the distance between the elements of the CCD matrix, it is necessary to ensure a resolution not lower than $1000\,mm^{-1}$. To obtain information on the object structure at the diffraction limit at a CCD pixel size of $13.4\,\mu m$ an optical magnification of over 20 object image diameters is needed. The resolving power of the recording system is mainly determined by the resolution of the IT. At the level of 20% the IT resolution is $20mm^{-1}$, which can be seen from the modulation transfer function (MTF) of the system IT + CCD (Fig. 5). The dots show the contrast values measured from the standard. The field of view of the speckle interferometer is defined by the size of the region of isoplanetism characteristic of BTA and is about 2″. For this reason the microobjective used for magnification must construct an aberration-free portion of the sky image with linear sizes of about $0.2\,mm$ in the focal plane of the telescope.

The device incorporates commercial microobjectives of the firm Karl-Zeiss. They are mounted on a linear displacement device providing the precision of no worse than $2\,\mu m$. The microobjectives give magnifications $2.5^{\times}$, $20^{\times}$ and $32^{\times}$. The field of view at the prime focus of the telescope at the given magnifications will be 26.″5 (scale 0.″052/pixel, 3.″3 (scale 0.″003/pixel and 2.″1 (scale 0.″004/pixel), respectively. The $32^{\times}$ magnification microobjective is mostly used in observations. The $20^{\times}$ magnification microobjective is employed on the nights with bad seeing when observing ultimately faint objects and broad pairs. The $2^{\times}$ magnification is intended to searching for an object and its positioning on the monitor center. It makes it possible to do without the TV guide television camera since the error of pointing the telescope does not exceed 5″.

3.5. Unit of light filters

The spectral band for recording images is formed by means of interference filters that are installed on one of the mechanisms of rotation, which are introduced sequentially in the beam of light by rotating the turel. The characteristics of the filters are presented in Fig. 6. Most commonly filters for wavelengths of 546, 610 and 800 nm and with a passband 30, 20 and 60 nm, respectively, are used. On the second mechanism of rotation there located the neutral filters to reduce light from bright sources and the devices for performing calibrations adjustment and investigation of the speckle-interferometer.

3.6. Shutter

To obtain images with short exposure an electromechanical fast action shutter of the type Uniblitz with an output opening of $6\,mm$ and a maximum frequency labour-rent of 200 Hz. The shutter ensures three working exposures 5, 10 and $20\,ms$. The moment of opening of the shutter is synchronized with the pulse of the beginning of exposure of the camera. The moment of closing of the shutter is chosen by the observer depending on the task and conditions. It is also possible to keep the shutter continuously opened or closed.

3.7. Compensator of atmospheric dispersion

Chromatism of the Earth atmosphere extends the image of a star into a spectrum elongated towards the zenith. The amount of chromatism depends on the zenith distance z of the object

$$\Delta z = (n_b - n_r)\mathrm{tg}\ z, \qquad (1)$$

where n_b and n_r are indices of refraction of air at short and long-way boundaries of the portion of the spectrum used. When observing, for instance, at

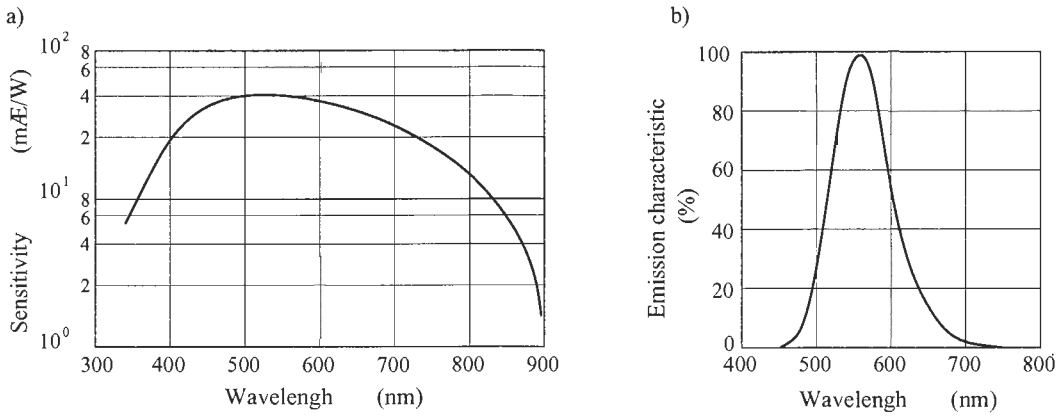

Figure 4: *Spectral sensitivity of the photocathode(a) and spectral characteristics of the luminophore (b).*

$z = 45°$ in a filter of width $\Delta\lambda = 20\,\text{nm}$, the size of the extended image is 3 times the characteristic size of the speckle for $\lambda = 600\,nm$. To preserve the angular resolution along the direction z, the atmospheric dispersion should be compensated for. The correction of atmospheric chromatism in SI is performed with the prism made of a pair of cemented wedges, which is placed in the beam f : 128 behind the microscope objective. The prism introduces in the image dispersion opposite in sign to atmospheric. The correction is made by moving the prism along the optical axis of the SI within the working section from the light filters to the input of the IT (the section length is $50\,mm$). The wedges of the prism are made of glasses SF L6 and La SF N30 with refraction indices 1.6128 and 1.6140. The dispersion curve of the prism is displayed in Fig. 7. The prism ensures the atmosphere dispersion correction in the spectral range 400–900 nm (in

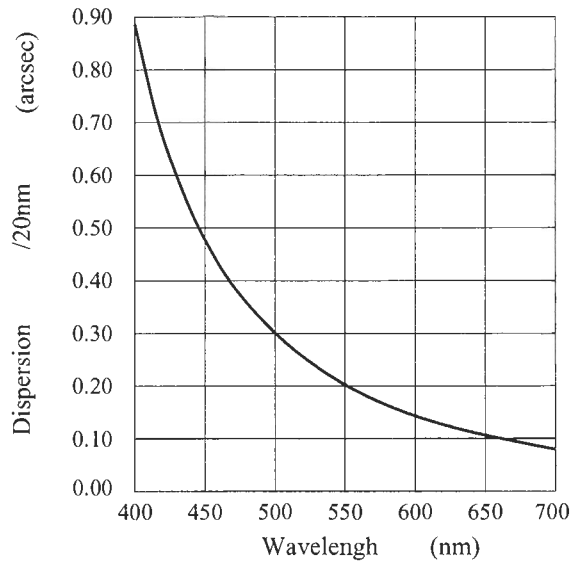

Figure 6: *Dispersion curve of the prism.*

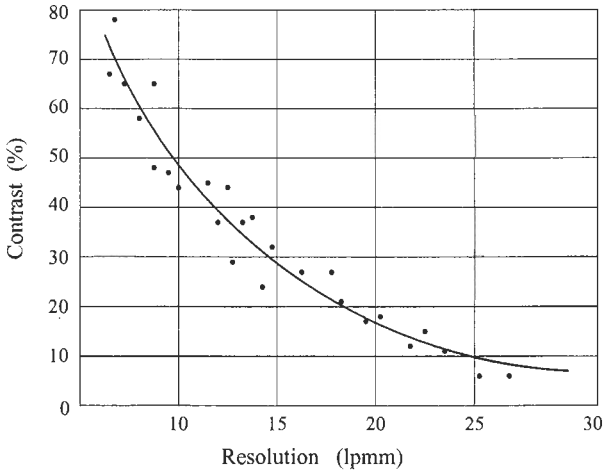

Figure 5: *MTF of the system IT + CCD.*

the band 20 nm) within the zenith distances $5° - 60°$. The calibration of the prism positions is made using observations of bright stars at different zenith distances. The setting of the prism into the calculated position is accomplished automatically by the coordinates of the stars.

3.8. The drive for the electromechanical units

The electromechanical units of the SI with optical elements installed on them are controlled by a specialized controller DC manufactured by the firm OWIS. The controller provides 9 modes of operation and control from the computer through standard interfaces RS-232 or LEEE-488. Manual control of the electromechanical units is also provided. The block

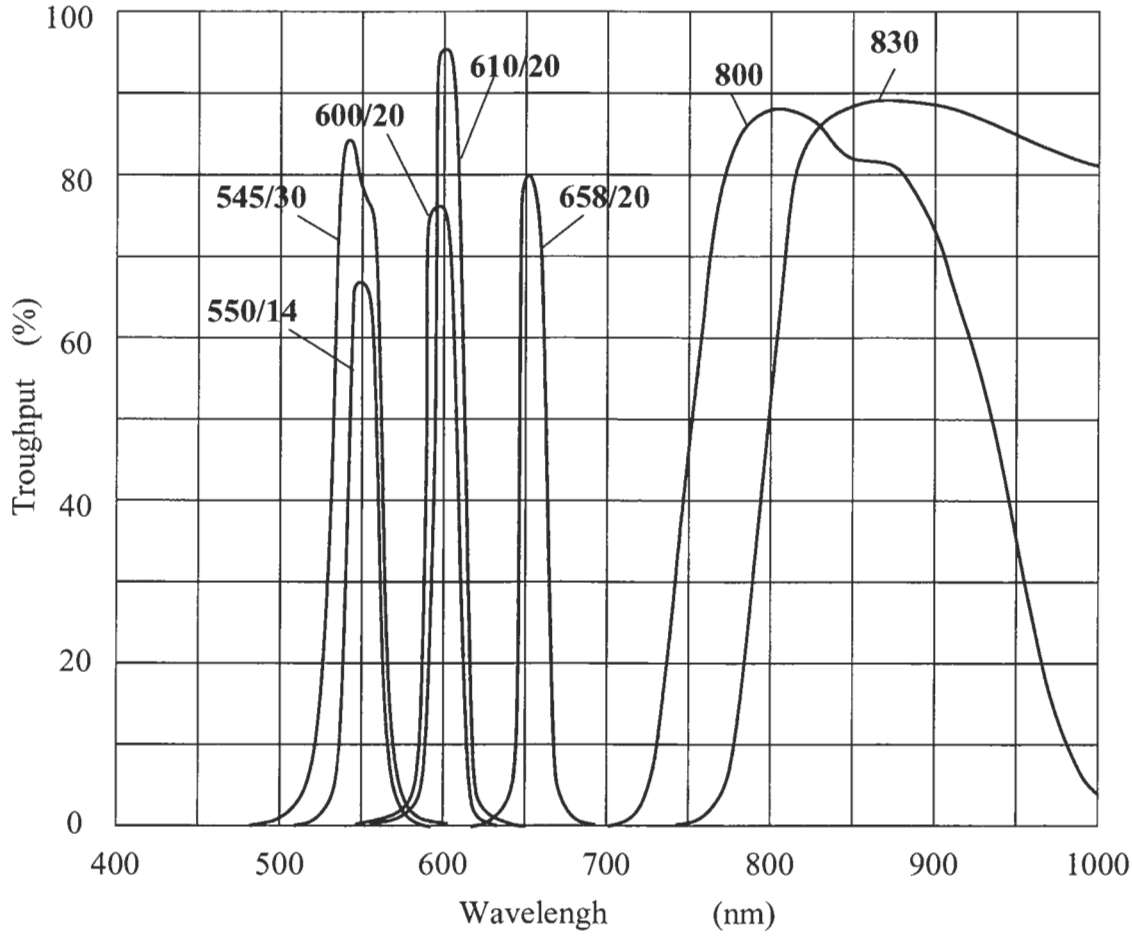

Figure 7: *Passbands of interference light filters.*

diagram of control of one of them is shown in Fig. 8.

The following units are included in the controller.

1. Microprocessor unit — processes the data from the computer and feedback signals from the sensors, form control signals.
2. Mode setting unit — specifies parameters for operation, reading out data from the patch board.
3. Indicator unit — represents input and current data on the LSD display of 4×40 symbols.
4. Power amplifiers (one for each mechanism) transform logical signals from the microprocessor unit to direct signals of 24 V, 2 A to control the motors.

As actuating mechanism, high precision mechanism of linear and circular displacement are employed, on which optical elements are placed. Each mechanism incorporates

- mechanical part consisting of a housing, precision guides, a micrometer screw and a carriage;
- direct current motor;
- digital feedback encoder of increment type, producing 500 pulses per revolution with a maximum inquiry frequency of 100 kHz.

The mechanism of circular displacement differs from the linear one only in its mechanical part. The mechanism uses a screw worm pair instead the micrometer screw. The precision of setting the optical elements is 1 to 5 μm.

3.9. The design

All the elements of the optical layout are located in all-metal housing made of aluminium alloy. To diminish the weight and ensure the required stiffness at the same time, the housing is provided with stiffening ribs all over. A flange is fixed to its front part, having a central hole to fasten the device at the focus of the telescope. To protect from diffused light, the housing is provided with blends and cutting off screens. Complete light insulation is achieved by installation of a non-transparent cover. Pillars are provided for fastening electronic units in the lower part of the housing.

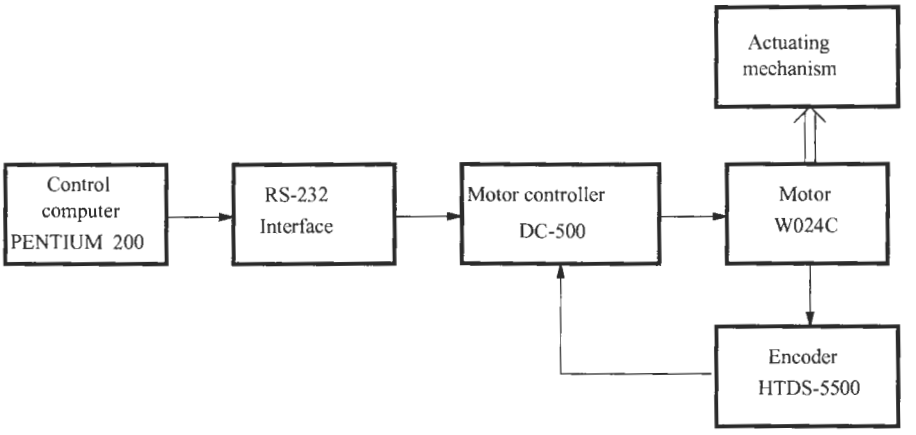

Figure 8: *Block-diagram of the controller.*

4. Observations and preprocessing of data.

Testing observations with the speckle interferometer were made at the 6 meter telescope SAO RAS on 12 December 1997. Some binary stars with large orbital periods and separations between $0''.02$ and $0''.7$ were selected as the objects (Table 1). The atmospheric seeing was about $3''$. From 300 to 2000 speckle images have been recorded for each star, depending on its brightness. The quantum efficiency of the system, based on S/N ratio of a single star power spectrum, turn to be equal 1.5%, 3.9% and 5.2% at spectral bands near 780 nm, 610 nm and 545 nm, respectively. It makes possible to observe stars as faint as 14^m, when seeing is better than $1''$(Balega et. al. 2002).

Preprocessing of speckle interferometric data include following steps:

1. Accumulation of flat field and dark signal of the camera and standard photometrical correction for each speckle interferometric image.

Because of noise emission of the intensifier, it is impossible to get a flat field estimation with usual bright sky using. Intensifier ionic events are concentrated near the frame center and damage the flat field. On the other hand, low amplitude noise events also affect the flat field estimation. These kinds of noise can be eliminated by accumulation of the flat field at low illumination on the photocathode. The flux must be chosen so low, that each event should be apart from other ones. The discrimination levels ε_{min} and ε_{max} to select noise events can be determined by using function $\varepsilon P(\varepsilon)$, where ε is photoelectron energy, and $P(\varepsilon)$ is number of photoelectrons distribution (Fig. 9). As an example, flat fields, obtained with usual bright sky using and with the method described above are presented in Fig. 10. Flat field of the speckle interferometer is characterized by high frequency inhomogeneities with rms fluctuation about 5% and low frequency decreasing of the sensitivity towards the field edge about 20%.

2. Selection of ionic events and cleaning of frames from ionic events.

Ionic events look on the IT like a bright flash with intensity often exceeding the dynamic range of the camera. The maximal level of photoelectronic events is about 200–250 counts of ADC (analog-to-digital converter), whereas the maximal intensity of ionics can reach maximal count of ADC, which is equal 4095. The number of ionic events is varied from 0 to 10 per frame. These ones make considerable contribution to power spectra or bispectra of speckle series and should be excluded from speckle images. The ionics can be easy selected in each frame, due to its energy. The cleaning procedure consists in replacement of the counts corresponding to the ionics by the mean image value in a small area near the event.

3. Selection of images by their position in the frame.

Because of telescope guiding errors some images are significantly shifted towards the edge of the frame. Such frames are not used for subsequent processing. We did not correct the geometrical distortions since in the working region the distortion is not high (no higher than 1%) and is not time variable.

5. Evaluation of power spectra. Measurement of parameters of binary stars

The simplest processing of speckle interferometric data consists in accumulation of the average power spectrum/autocorrelation function of a series of instantaneous images of the object

$$\langle|\widetilde{I}(\boldsymbol{\nu})|^2\rangle = |\widetilde{O}(\boldsymbol{\nu})|^2\langle\widetilde{S}^{(2)}(\boldsymbol{\nu})\rangle + \widetilde{N}(\boldsymbol{\nu}), \qquad (2)$$

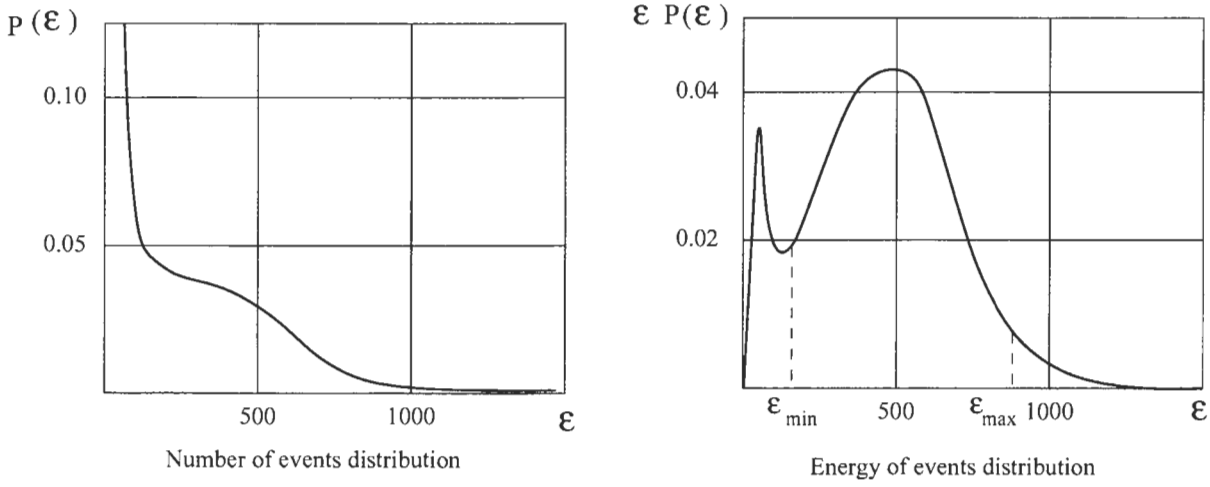

Figure 9: *Amplitude distributions of photon events.*

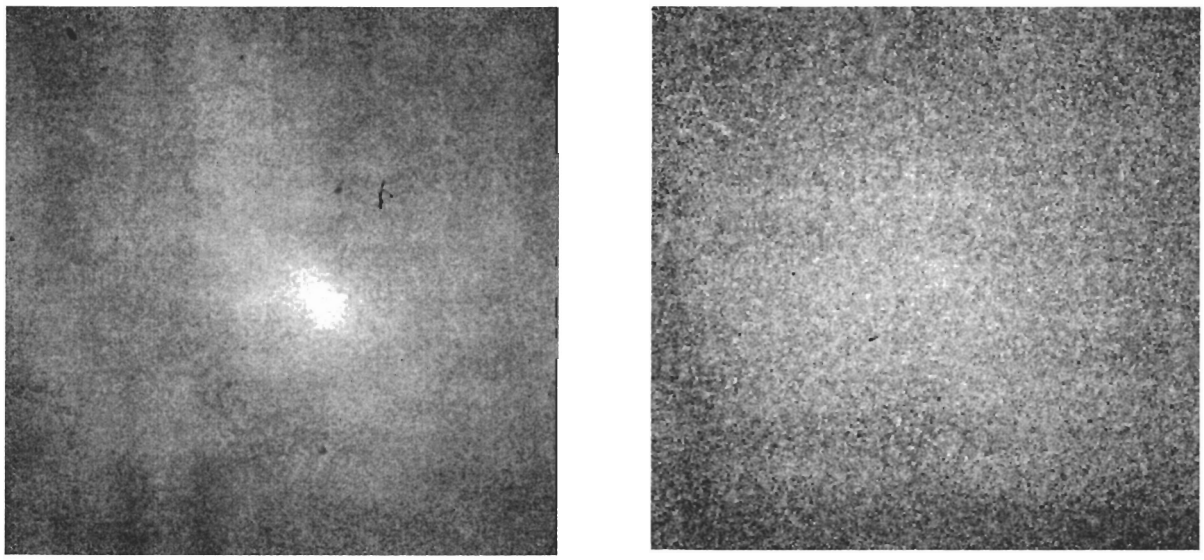

Figure 10: *Frame of homogeneous illumination before a) and after b) the subtraction of multielectron scintillations.*

where $\boldsymbol{\nu}$ is spatial frequency, $\langle |I(\boldsymbol{\nu})|^2 \rangle$ is the average object power spectrum, $|O(\boldsymbol{\nu})|^2$ – is the square of the object spartial spectrum, $\langle |S(\boldsymbol{\nu})|^2 \rangle$ is the average power spectrum of the point source, and $\widetilde{N}(\boldsymbol{\nu})$ is the power spectrum of the noise.

In the case of the 6 meter telescope, the first term in (2) can be described by Korff model (Korff 1973)

$$\langle \widetilde{S}^{(2)}(\boldsymbol{\nu}) \rangle = \widetilde{T}_0^2(\boldsymbol{\nu}) e^{-6.88(\lambda\nu F/r_0)^{\frac{5}{3}}[1-(\lambda\nu F/D)^{\frac{1}{3}}]} + 0.435(r_0/D)^2 \widetilde{T}_0(\boldsymbol{\nu}), \quad (3)$$

where $\widetilde{T}_0(\boldsymbol{\nu})$ is the MTF of an aberration-free telescope.

Photon bias and detector noise predominately contribute to the function $N(\nu) = N_p(\nu) + N_d(\nu)$. The effect of detector noise $N_d(\nu)$ is quite low in comparison with the photon bias term $N_p(\nu) = C_p n_p(\nu)$. Its power spectrum is estimated using a set of dark signal frames, renormalized according to the number of frames and substracted from the object power spectrum. The normalized photon bias term $n_p(\nu)$ depends on the shape of photon events and is same as

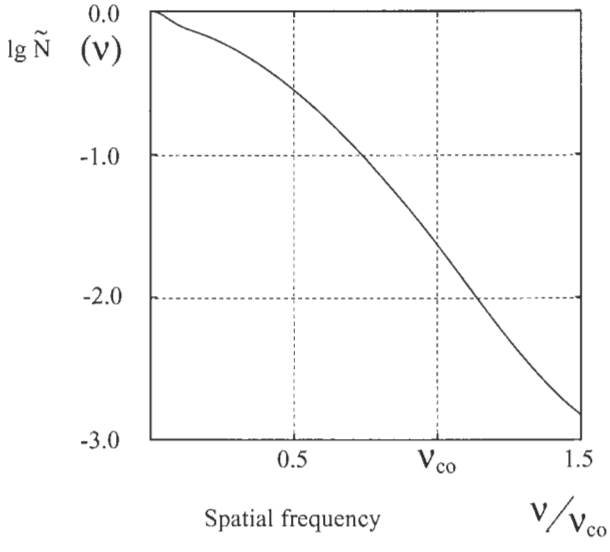

Figure 11: *Spectral power of photon noise*

square of the detector MTF. The MTF is quite time stable and can be obtained as normalized power spectrum of flat field frames (Fig. 11). Photon bias amplitude C_p can be obtained from the object power spectrum beyond the telescope cut-off frequency, where the object signal is equal to zero. To correct residuals after the noise bias correction we used an iterative algorithm, which is described below.

Let us define a weighting function $V(r)$ as

$$V(r) = e^{-\frac{r^2}{\sigma_m^2}}, \tag{4}$$

where r is the distance to the center of the object autocorrelation function, and σ_m is the parameter, which defines the width of the $V(r)$. Let us define $\langle \tilde{I}_j^{(2)}(\boldsymbol{\nu}) \rangle$ as the j-th approximation of the average power spectrum of the object. The next estimation of the autocorrelation function $\langle I_{j+1}^{(2)}(\mathbf{r}) \rangle$ can be calculated from equation

$$\langle I_{j+1}^{(2)}(\mathbf{r}) \rangle = \begin{cases} F_j(\mathbf{r}) & F_j(\mathbf{r}) > 0, \\ 0 & F_j(\mathbf{r}) \le 0, \end{cases} \tag{5}$$

where $F_j(\mathbf{r}) = V(r)\, I_j^{(2)}(\mathbf{r}) + (1 - V(r))\, \langle I^{(2)}(\mathbf{r}) \rangle$, $I^{(2)}(\mathbf{r})$ is the average autocorrelation function of the object, and $I_j^{(2)}(\mathbf{r})$ is the autocorrelation function associated with the power spectrum

$$\tilde{I}^{(2)}(\boldsymbol{\nu}) = \begin{cases} \langle \tilde{I}_j^{(2)}(\boldsymbol{\nu}) \rangle & \nu < \nu, \\ 0 & \nu > \nu. \end{cases} \tag{6}$$

Fourier transform of the function $\langle I_{j+1}^{(2)}(\mathbf{r}) \rangle$ is used as the next estimation of the power spectrum $\langle \tilde{I}_{j+1}^{(2)}(\boldsymbol{\nu}) \rangle$. The average power spectrum of the object with substracted noise bias term is used as the null approximation. The iteration is conducted for increasing set of σ_m. The σ_m values are changed from 0 to the maximal value, which is equal to the typical size of the photon event. Changing from σ_m to σ_{m+1} occure when the difference between the next two approximation of the autocorrelation function will be negligible small. The algorithm converges to the positive function, which is practically the same as the object autocorrelation function in the region where bias caused by the noise is negligible. The spatial spectrum of the solution is equal 0 beyond the cut-off frequency of the telescope.

The contribution of the low-frequency part of the speckle interferometric transfer function (the first term in eq. (3)) can be considerably decrease by accumulation of the power spectrum of the differences of the speckle images. The accumulation corrects both dark signal and the effects of the camera afterglow. Low-frequency residuals after such averaging can be corrected with the algorithm very similar to the noise bias correction algorithm described above.

Autocorrelation functions $\langle I^{(2)}(\mathbf{r}) \rangle$, obtained with described approach (Fig. 12), have been used to derive positional parameters of the stars by measuring of autocorrelation peaks positions.

The accuracy of position measurements for different pairs varied within the range $0''.001 - 0''.004$ in ρ and $0.^\circ 2 - 3^\circ$ in θ, depending on the brightness and seeing. The measurement results are collected in Table 1.

Some examples of autocorrelation functions power spectra of binaries are presented on Fig. 13–16.

The star HIP 25354 was first resolved by the astrometric satellite Hipparcos in 1991.25 as a binary. The spectral class is K8, the stellar magnitude is $10^m.37$. After the processing of speckle interferometric data of the 1999.81 observations, a faint 3rd component was discovered in the system (in Fig. 13 it is indicated by an arrow). Since the difference in brightness between the components of the system is considerable, the ACF, but not the power spectrum is presented in the figure.

For the binary HIP 20227 of spectral class GS and m = 8.7 the difference in luminosity between the components is $\Delta m = 3.6$. In this case it is also expedient to give as an illustration the ACF, but not the power spectrum (Fig. 14).

The potentialities of the method to obtain parameters of wide pairs can be illustrated by the example of autocorrelation for the system HIP 94960 of spectral class MO and $m_V = 10.2$. The distance between the components at the moment of separation was $\rho = 0''.479$ (Fig. 15).

As an example of resolution of a most close pair of stars, Fig. 16 displays the power spectrum of the spectral binary Chara 126 of class G2III+F2N, stellar magnitude $5^m.8$. The distance between the compo-

Table 1: *Results of measurements of binary stars with the new speckle interferometer of BTA.*

Name	Coordinates 2000	Date 1997.0+	Spectral range (nm)	ρ''	θ°
HBC 36	04271+2543	.9692	658/20		
ADS 3475	04512+1104	.9691	610/20	0.260	58.5
+22 0818	05056+2304	.9691	600/20	0.373	151.4
ADS 4660	06052+0708	.9691	610/20	0.457	42.7
ADS 4660	06052+0708	.9692	610/20	0.457	42.9
ADS 4950	06221+5922	.9692	610/20	0.689	139.9
+31 1684	07535+3038	.9695	610/20		
HR 3109	08017+6019	.9692	610/20	0.098	303.7
ADS 6578	08071+5407	.9693	610/20	0.412	206.1
ADS 6993	08468+0625	.9694	658/07	0.280	183.6
HR 3750	09278-0604	.9693	600/20	0.510	332.6
+11 2252	10367+1101	.9694	658/20	0.105	251.3
+21 2247	10515+2017	.9694	610/20		
+29 2110	11008+2913	.9693	610/20	0.210	108.5
ADS 8535	12238+5410	.9696	610/20	0.395	261.7
+10 2617	14025+0941	.9695	610/20		
41 Dra	18002+8000	.9696	610/20	0.024	341.2

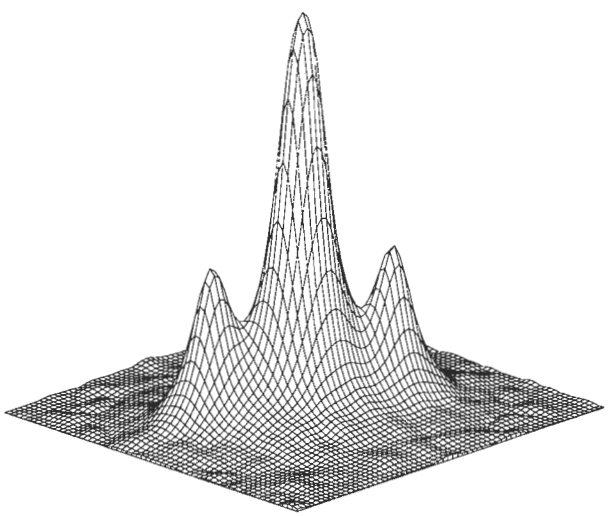

Figure 12: *ACF of the binary star 53 Cam.*

nents of this system is 0.″025.

6. Reconstruction of images

It is necessary to know both amplitudes $|\widetilde{O}(\boldsymbol{\nu})|$ and Fourier phases $\varphi(\boldsymbol{\nu})$ to reconstruct the diffraction limited image of the object from its spatial spectrum. At the present time bispectral method (Weigelt 1991) is the common way to obtain the spatial spectrum phases of the object. An unbiased estimate of the mean bispectrum of the object is given by the expression (with no allowance for the average profile of the photon flash) (Pehlemann et. al. 1992):

$$\begin{aligned}\langle\widetilde{I}^{(3)}(\boldsymbol{\nu}_1,\boldsymbol{\nu}_2)\rangle &= \langle\widetilde{I}(\boldsymbol{\nu}_1)\widetilde{I}(\boldsymbol{\nu}_2)\widetilde{I}(-\boldsymbol{\nu}_1-\boldsymbol{\nu}_2)\rangle - \\ &\quad C_1(\widetilde{I}^{(2)}(\boldsymbol{\nu}_1)+\widetilde{I}^{(2)}(\boldsymbol{\nu}_2)+ \\ &\quad \widetilde{I}^{(2)}(-\boldsymbol{\nu}_1-\boldsymbol{\nu}_2)) - C_2 - \\ &\quad \langle\widetilde{G}(\boldsymbol{\nu}_1)\widetilde{G}(\boldsymbol{\nu}_2)\widetilde{G}(-\boldsymbol{\nu}_1-\boldsymbol{\nu}_2)\rangle, \quad (7)\end{aligned}$$

where $\langle\widetilde{G}(\boldsymbol{\nu}_1)\widetilde{G}(\boldsymbol{\nu}_2)\widetilde{G}(-\boldsymbol{\nu}_1-\boldsymbol{\nu}_2)\rangle$ is the mean bispectrum of the detector noise, and $\widetilde{I}^{(2)}(\boldsymbol{\nu})$ is the unbiased estimation of the object power spectrum. Normalizing constants C_1 and C_2 can be derived from the bispectrum values if one of spatial frequences ν_1, ν_2, and $|-\boldsymbol{\nu}_1-\boldsymbol{\nu}_2|$ are higher than the telescope cutoff limit. The phase of the mean bispectrum is not distorted by the atmosphere and then

$$\arg[\langle\widetilde{I}^{(3)}(\boldsymbol{\nu}_1,\boldsymbol{\nu}_2)\rangle] = \arg[\widetilde{O}(\boldsymbol{\nu}_1)\widetilde{O}(\boldsymbol{\nu}_2)\widetilde{O}(-\boldsymbol{\nu}_1-\boldsymbol{\nu}_2)]. \quad (8)$$

The reconstruction of spatial spectrum phases of the object $\varphi(\boldsymbol{\nu})$ by the phase of its bispectrum $\arg[\widetilde{O}(\boldsymbol{\nu}_1)\widetilde{O}(\boldsymbol{\nu}_2)\widetilde{O}(-\boldsymbol{\nu}_1-\boldsymbol{\nu}_2)]$ is executed with the aid of a recursive procedure with subsequent use of iterative algorithm for phase restoration (Hofmann et. al. 1990).

7. Conclusions

The new digital speckle interferometer improved drastically results being obtained. The following advantages of the system described should be noted.

1. The new device has considerably higher sensitivity, resolution and dynamical range in comparison with its prototype.

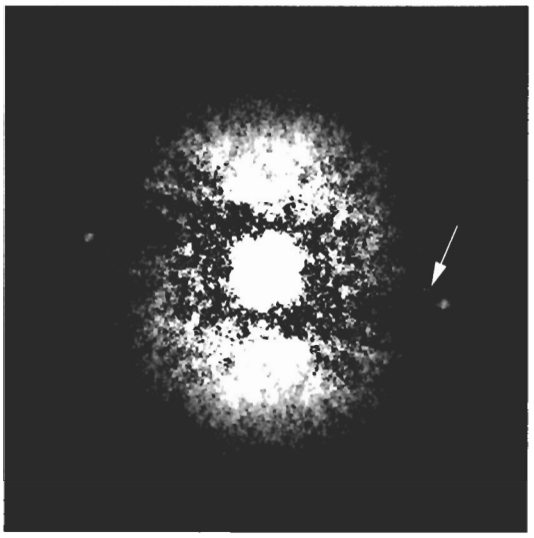

Figure 13: *ACF of the star hip25354.*

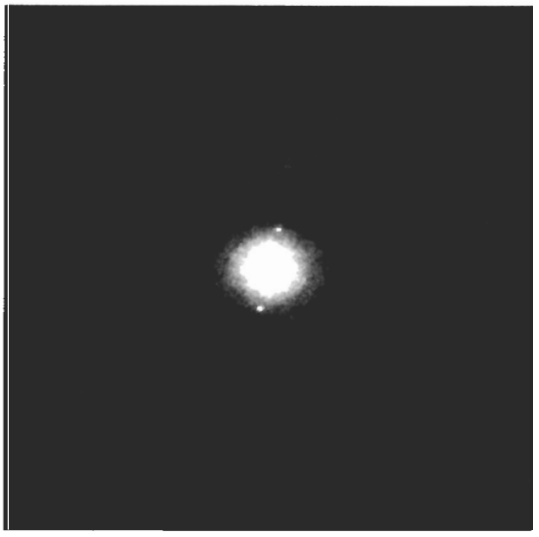

Figure 14: *ACF of the star hip20227.*

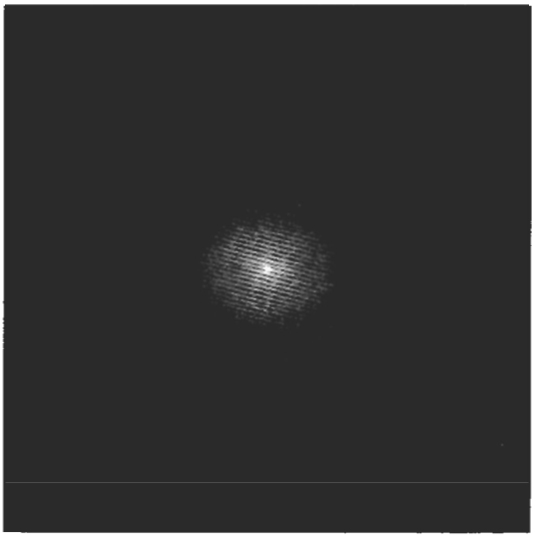

Figure 15: *Power spectrum of the object hip94960.*

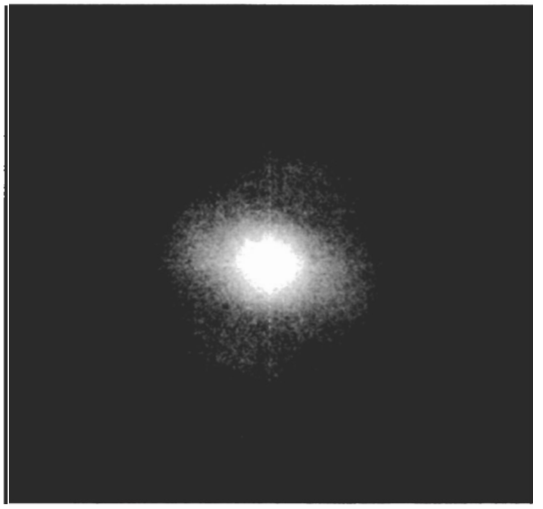

Figure 16: *Power spectrum of the star Chara126.*

2. The replacement of the television camera based on the vacuum tube by a CCD system enabled improvement of stability of electric parameters and reproduction of results.

3. The use of fiber-optical communication lines eliminated completely the influence of external electromagnetic interferences and increased the speed of data transmission.

4. The change from the mode of centering to the complete analog-to-digital conversion of a frame made it possible remove the non-linearity of recording close photon events, which is of prime importance for performing the tasks of image reconstruction.

5. The operation at a specified high voltage and minimized tunings of the device simplified the procedure of calibrations.

6. The need for the presence of the observer at the prime focus of BTA is in the process of observations eliminated. All operations on handling optical and mechanical elements and changing the conditions of operation of the device are executed remotely from the control room.

7. The adjustment and tuning of the apparatus is conducted under laboratory conditions.

At the same time, it should be noted that as yet the problem of data transmission to external media has not been solved completely. Under the control

of the program SensiCam in the operational environment Windows 95 the speed of data transmission is no higher than 6 frames/s at a maximum possible flow from the camera of 8 frames/s. In observations, depending on the condition of data recording on a specific carrier, the speed is still lower and makes 3–5 frames/s.

References

Balega Y.Y., Somov N.N., Fomenko A.F., 1981, Astrofiz. Issled. (Izv. SAO), **14**, 138

Balega Y.Y., Ryadchenko V.P., 1984, Pis'ma Astron. Zh., **10**, 229

Balega I.I., Balega Y.Y., Hofmann K.-H., Maximov A.F., Pluzhnik E.A, 2002, Astron. Astrophys., **385**, 89

Weigelt G., 1991, in: Progress in optics, ed. E. Wolf, 295

Dudinov V.N, Erohin V.N., Kuzmenkov S.G., Rilov V.S., Cvetkova V.S., Shabanov M.F., 1979., Dokl. UkrSSR, ser.A7, 550

Korff D., 1973, J. Opt. Soc. Am., **63**, 971

Labeyrie A., 1970, Astron. Astrophys., **6**, 85

Nakajima T., Kulkarni S.R., Gorham P.W., Ghez A.M., Neugebauer G., Oke J.B., Prince T.A., Readhead A.C.S., 1989, Astron. J., **97**, 1510

Papaliolios C., Nisenson P., Ebstein S., 1985, Appl. Opt., **24**, 287

Timothy J., 1983, Publ. Astr. Soc. Pacific, **106**

Horch E., Heanue J.F., Morgan J.S., Timothy J.G., 1994, Publ. Astr. Soc. Pacific, **106**, 992

Pehlemann E., Hofmann K-H., Weigelt G., 1992, Astron. Astrophys., **256**, 701

Hofmann K-H., Weigelt G., 1990, in: SPIE Proc., Digital image synthesis and inverse optics, San Diego, CA, July 9-13, 522